

HyperLips: Hyper Control Lips with High Resolution Decoder for Talking Face Generation

Yaosen Chen, Yu Yao, Zhiqiang Li, Wei Wang, Yanru Zhang, Han Yang, Xuming Wen

Abstract—Talking face generation has a wide range of potential applications in the field of virtual digital humans. However, rendering high-fidelity facial video while ensuring lip synchronization is still a challenge for existing audio-driven talking face generation approaches. To address this issue, we propose HyperLips, a two-stage framework consisting of a hypernetwork for controlling lips and a high-resolution decoder for rendering high-fidelity faces. In the first stage, we construct a base face generation network that uses the hypernetwork to control the encoding latent code of the visual face information over audio. First, FaceEncoder is used to obtain latent code by extracting features from the visual face information taken from the video source containing the face frame. Then, HyperConv, which weighting parameters are updated by HyperNet with the audio features as input, will modify the latent code to synchronize the lip movement with the audio. Finally, FaceDecoder will decode the modified and synchronized latent code into visual face content. In the second stage, we obtain higher quality face videos through a high-resolution decoder. To further improve the quality of face generation, we trained a high-resolution decoder, HRDecoder, using face images and detected sketches generated from the first stage as input. Extensive quantitative and qualitative experiments show that our method outperforms state-of-the-art work with more realistic, high-fidelity, and lip synchronization. Project page: https://semchan.github.io/HyperLips_Project/

Index Terms—Talking face generation, hypernetwork, lip synchronization, high-fidelity faces.

I. INTRODUCTION

WITH the growth of audio-visual content [1]–[6] and the rise of the metaverse, talking face generation has broad application prospects in visual dubbing [7]–[9], digital assistant [10], virtual human [11], animation film and other fields, and has attracted more and more attention.

Based on the input requirements of the application, talking face generation methods can be categorized as driving audio

Yaosen Chen is with University of Electronic Science and Technology of China, Chengdu, Sichuan, 611731 China, and also with Media Intelligence Laboratory, ChengDu Sobey Digital Technology Co., Ltd, Chengdu, Sichuan, 610041 China e-mail: (chenyaosen@sobey.com).

Yu Yao and Zhiqiang are with Media Intelligence Laboratory, ChengDu Sobey Digital Technology Co., Ltd, Chengdu, Sichuan, 610041 China, e-mail: (yaoyu, lizhiqiang@sobey.com).

Wei Wang is with Media Intelligence Laboratory, Chengdu Sobey Digital Technology Co., Ltd, Chengdu, Sichuan, 610041, China, and also with Peng Cheng Laboratory, Shenzhen 518055, China e-mail: (wangwei@sobey.com).

Yanru Zhang is with University of Electronic Science and Technology of China, Chengdu, Sichuan, 611731 China e-mail: (yanruzhang@uestc.edu.cn).

Han Yang is with University of Electronic Science and Technology of China, Chengdu, Sichuan, 611731 China, and also with Media Intelligence Laboratory, ChengDu Sobey Digital Technology Co., Ltd, Chengdu, Sichuan, 610041 China e-mail: (yanghan@sobey.com).

Xuming Wen is with Media Intelligence Laboratory, Chengdu Sobey Digital Technology Co., Ltd, Chengdu, Sichuan, 610041, China, and also with Peng Cheng Laboratory, Shenzhen 518055, China e-mail: (wenxuming@sobey.com).

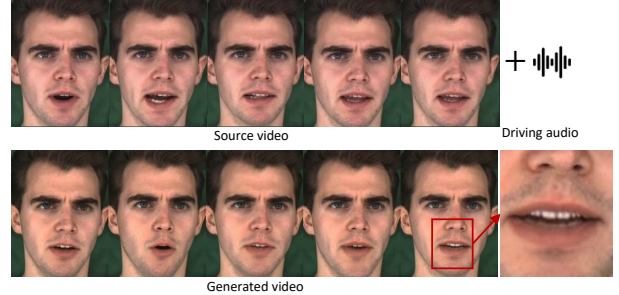


Fig. 1. Given the visual face information of source videos (upper left) and driving audio (upper right), our method is capable of rendering and generating more realistic, high-fidelity, and lip-synchronized videos (lower). See the zoom-in patches, our method can see details such as teeth.

only [12]–[16], driving audio with a single frame [17]–[19], and driving audio with source video (or multiple frames) [8], [20]–[23] types. For driving audio only, it is person-specific primarily and requires re-training for videos captured by the target speaker. For example, using a neural radiance field to train the implicit 3D representation of a captured video of a specific speaking person can observe the person’s speech in a novel view [12], [13], but the rendering results always look unnatural during movement. Due to the lack of facial and motion information as input for driving audio with a single frame, although some studies have done enough work, it is still impossible to generate accurate expressions and natural motion sequences [18]. For driving audio with source video, as shown in Fig. 1, the expressions and movements of the characters in the generated video are mostly taken from the source video, which naturally has realistic expressions and natural movements. In this case, there are two main challenges: 1. How to produce more accurate **lip synchronization** in generated videos; 2. How to render more **high-fidelity** faces, especially high-definition lips and teeth, in generated videos. To produce more accurate lip synchronization in generated videos, Wav2lip [8] proposed a lip sync discriminator to improve the performance of lip synchronization in unconstrained videos; SyncTalkFace [20] proposed an audio lip memory that uses visual information of the mouth region corresponding to the input audio and enforces fine-grained audio-visual coherence; IP_LAP [21] leveraged a transformer-based landmark generator to infer lip and jaw landmarks from the audio to synchronize lip shape. These methods typically fuse the visual and audio features before decoding. However, the dimensions of audio and visual features are different, so additional processing is required to make them the same size for feature fusion. In the first stage of our method, we encode visual face information as a latent code,

then modify the latent code by a HyperConv convolution operation, and finally decode the modified latent code into visual face content. The weight parameters of HyperConv are generated by constructing a hypernetwork using audio features as input, thus achieving audio control of lip movement in the rendered visual content. We use hypernetwork to avoid additional operations during the fusion of visual and audio features and to ensure lip synchronization in the generated videos better. Our idea is similar to the Audio Conditioned Diffusion Model [24], which takes audio information as the condition variable. Still, this method takes the diffusion model as the network architecture, which increases the demand for computational resources.

To render more high-fidelity faces, DINet [22] proposed a Deformation Inpainting Network to achieve face visually dubbing on high-resolution videos, but it may generate artifacts out of face if mouth region covers background. IP_LAP [21] leverage the prior appearance information which is extracted from the lower-half occluded target face and static reference images, it may fail when landmark cannot be detected in the reference images. Another possible method is to increase the input resolution based on networks such as Wav2lip [8] or SyncTalkFace [20], but this not only increases the need for training resources but also does not render well, resulting in persistent artifacts. In the second stage of our method, we propose a high-resolution decoder (HRDecoder) to further optimize the fidelity of generating faces. We trained the network using the facial data generated in the first stage and the corresponding facial sketches, guided by the sketches, to achieve facial enhancement.

In summary, the contributions of our work are as follows:

- We propose a hypernetwork based on audio information to control the generation of facial visual content that improves lip synchronization.
- We propose a high-resolution decoder with facial sketch guidance that can render more high-fidelity faces, especially high-definition lips and teeth, in generated videos.
- Extensive experiments show that our method can achieve significantly better talking face generation performance in terms of lip synchronization and face quality.

II. RELATED WORK

A. Audio-Driven Talking Face Generation

In methods that only use audio input for audio-driven talking face generation [12]–[16], collecting audio and video for person-specific and re-training is usually necessary. By introducing a neural radiance field (NeRF) [25] to represent the scenes of talking heads [13], it can be controlled to render the face in a novel view. RAD-NeRF [12] decompose the inherently high-dimensional talking portrait representation into three low-dimensional feature grids, that makes can rendering the talking portrait in real-time. GeneFace [14] propose a variational motion generator to generate accurate and expressive facial landmark and uses a NeRF-based renderer to render high-fidelity frames. Due to a lack of prior information, these tasks still struggle to render realistic expressions and natural movements. To drive a single facial image, ATVGnet [17]

devises a cascade GAN approach to generate a talking face video, which is robust to different face shapes, view angles, facial characteristics, and noisy audio conditions. Recently, SadTalker [18] propose a novel system for a stylized audio-driven single-image talking face animation using the generated realistic 3D motion coefficients, improving motion synchronization and video quality, but it is still impossible to generate accurate expressions and natural motion sequences. The method of driving audio with source video is the most competitive because it can provide enough realistic facial expressions and natural movement information. Wav2lip [8], SyncTalkFace [20], IP_LAP [21], DINet [22] all belong to this category, mainly focusing on how to generate better lip synchronization and higher fidelity faces.

B. HyperNetwork

Hypernetwork [26] was originally proposed to generate the weights for a larger network. In evolutionary computation, operating directly on large search spaces consisting of millions of weight parameters is difficult. A more efficient method is to evolve a smaller network to generate the weight structure for a larger network, so that the search is constrained to the much smaller weight space. The idea of weight generation is easy to use for controllable generation tasks. Chiang et al. [27] leverage it to control the style of the 3d scene representation. UPST-NeRF [28] uses hypernetwork to control the universal photorealistic style transfer for 3D scene. With the rise of Large Language Models (LLMs) [29]–[32] and generative models [33], hypernetwork has also become one of the necessary skills for fine-tuning LLMs. Essentially, the idea of generating weight parameters in a hypernetwork to control the large network method is similar to the Audio Conditioned Diffusion Model [24] and the Conditioning Mechanisms in Latent Diffusion Models [33], both of which achieve controllable output of the decoding through a control variable. In our method, however, we perform controllable generation relatively simply rather than using the diffusion model for generation. Wang et al [34] use hypernetwork for the application of magnetic resonance imaging reconstruction.

C. Prior Based Face Restoration

Face restoration is to restore the high-quality face image from the degraded face image [35]. Face restoration is divided Non-prior and Prior based methods. FSRNet [36] uses a coarse Super-Resolution (SR) network to recover coarse images, which are then processed by a fine SR encoder and a prior face-passing map estimation network, respectively. Finally, image features and prior information are fed to the fine SR decoder to get the results. In [37], it uses the semantic label as the face prior. The semantic label is extracted from the input image or coarse deblurred image by a face parsing network. The final sharp image is generated from a deburring network with the input of the concatenation of the blurred image and the face semantic label. Yin et al. [38] propose a joint alignment and face super-resolution network to learn landmark localization and face restoration jointly. In our work,

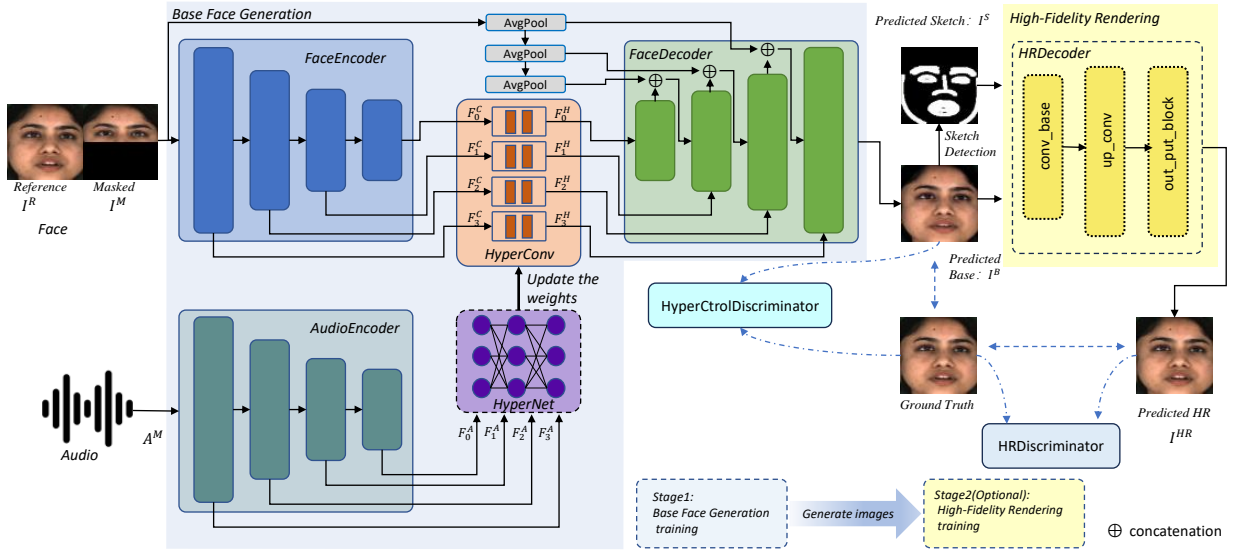


Fig. 2. Overview of our proposed model. It can be divided into two stages: **(1) Base Face Generation.** FaceEncoder encode the visual face information (Reference and Masked) as a latent code, then modify the latent code by a HyperConv convolution operation, and finally FaceDecoder decode the modified latent code into visual face content. The weight parameters of HyperConv are updated by a hypernetwork using audio features as input, thus achieving audio control of lip movement in the rendered visual face content (Base Face). **(2) High-Fidelity Rendering .** The high-resolution decoder (HRDecoder) is used to further optimize the fidelity of generating faces. We trained the network using the facial data generated in the first stage and the corresponding facial sketches, guided by the sketches, to achieve facial enhancement. Therefore, the input to HRDecoder is the concatenation feature of the base face with the sketch extracted from the base face, and the output is the high-fidelity face.

we use the landmark sketches detected from the relatively low-quality face generated in the first stage as input to guide the HRDecoder to achieve face enhancement to render high-fidelity faces.

III. PROPOSED METHOD

The overview of our framework is shown in Fig. 2. We aim to generate a high-fidelity talking face video with synchronized lip movements by implementing the occluded face in the lower half of the input video frame by frame, given an audio and video sequence. Our proposed method consists of two stages: Base Face Generation and High Fidelity Rendering. In Base Face Generation, we designed a hypernetwork that takes audio features as input to control the encoding and decoding of visual information to obtain base face images. In high-fidelity rendering, we trained an HRDecoder network using face data from the network trained in the first stage and corresponding face sketches to enhance the base face.

A. Base Face Generation

1) *Hyper Control Lips:* Given the reference image $I^R \in \mathbb{R}^{3 \times H^I \times W^I}$ and the masked image (occluded face in the lower half of the reference image) $I^M \in \mathbb{R}^{3 \times H^I \times W^I}$, FaceEncoder obtains the latent code $L^C = \{F_i^C\} | 0 \leq i \leq 3$ by extracting the I^R and I^M concatenation as inputs. Next, we use HyperConv's convolution operation to process L^C and obtain $L^H = \{F_i^H\} | 0 \leq i \leq 3$. Finally, we decoded L^H with FaceDecoder to get the predicted base face $I^B \in \mathbb{R}^{3 \times H \times W}$. The HyperConv implicit function can be formulated as follows:

$$\mathcal{F}_\Theta : (L^C) \rightarrow (L^H), \quad (1)$$

where Θ is the weight parameter of the HyperConv convolution operation, which predicated by the HyperNet. HyperNet is composed of MLP, with audio deep features $\{F_i^A\} | 0 \leq i \leq 3$ extracted by AudioEncoder as input. For the input of AudioEncoder, we follow [8] to extract the Mel-spectrogram of the audio as $A^M \in \mathbb{R}^{H^A \times W^A}$.

The size of the audio mel-spectrogram is usually 16×80 , i.e., $H^A=16$ and $W^A=80$. In contrast, the image size is usually not the same as the size of the audio mel-spectrogram, i.e., $H^I=W^I=128$ as default in our method. In our method, we do not need to unify the dimensions of audio features and visual features, so no additional operations are required compared to other methods.

2) *Loss Function for Base Face Generation:* To be competitive in lip synchronization and fidelity, we constrain the generated base face by integrating multiple losses. We adopt its architecture from [8] to design a quality discriminator which we called HyperCtrlDiscriminator, indicates as \mathcal{D}^B . Therefore, the overall generation process can be formulated as follows:

$$I^B = \mathcal{G}^B((I^R \oplus I^M), A^M), \quad (2)$$

where, \oplus indicate concatenation. In this way, we can consider the base face generation as a generator, indicates as \mathcal{G}^B , consisting of the following modules: FaceEncoder, HyperConv, FaceDecoder, AudioEncoder and HyperNet. We train the discriminator by adding the following loss:

$$\mathcal{L}_d^B = \mathbb{E}_{I^{GT}}[\log(1 - \mathcal{D}^B(I^{GT}))] + \mathbb{E}_{I^B}[\log(\mathcal{D}^B(I^B))], \quad (3)$$

Base Adversarial Loss: We employ the adversarial loss to constrain the realism of our generated images:

$$\mathcal{L}_a^B = \mathbb{E}_{I^B}[\log(1 - \mathcal{D}^B(I^B))], \quad (4)$$

Base Reconstruction Loss: We achieve visual reconstruction by constraining the l1 loss between the generated base face and the Ground Truth:

$$\mathcal{L}_r^B = \frac{1}{N} \sum_{i=1}^N \|I^B - I^{GT}\|_1, \quad (5)$$

Base LPIPS Loss: We employ the Learned Perceptual Image Patch Similarity loss [39] to constrain the generated images:

$$\mathcal{L}_l^B = \frac{1}{N} \sum_{i=1}^N LPIPS(I^B, I^{GT}), \quad (6)$$

Base Audio-Visual Sync Loss: We follow [20] use the audio-visual sync module proposed in [8], [40]. We train the audio-visual sync module, \mathcal{F}^A and \mathcal{F}^V , on LRS2 [41] datasets and no fine-tune on any generated frames. The generated 5 frames (lower half only) correspond to one audio segment, and the features obtained by \mathcal{F}^A and \mathcal{F}^V are represented as f_a and f_v , respectively. The outputs features' binary cross-entropy of cosine similarity is computed as follows:

$$d_{sync}(f_a, f_v) = \frac{f_a \cdot f_v}{\|f_a\|_2 \cdot \|f_v\|_2}, \quad (7)$$

The Audio-Visual Sync Loss can be formulated as:

$$\mathcal{L}_{av}^B = -\frac{1}{N} \sum_{i=1}^N (\log(d_{sync}(\mathcal{F}^A(A_i^M), \mathcal{F}^V(\mathbf{I}_i^B))))), \quad (8)$$

where $\mathbf{I}_i^B = \{I_n^B\}_{n=i-2}^{i+2}$.

To summarize, the training loss for the base face generation stage can be formulated as follows:

$$\mathcal{L}_{total}^B = \lambda_a^B \mathcal{L}_a^B + \lambda_r^B \mathcal{L}_r^B + \lambda_l^B \mathcal{L}_l^B + \lambda_{av}^B \mathcal{L}_{av}^B, \quad (9)$$

where λ_a^B , λ_r^B , λ_l^B , λ_{av}^B are the hyper-parameter weights.

B. High-Fidelity Rendering

1) *HRDecoder:* We have constructed a relatively simple High-Resolution Decoder (HRDecoder) consisting of a base convolution module, an upsampling convolution module, and an output convolution block. The transposed convolution in the upsampling convolution module can convert lower resolution features to higher resolution features. HRDecoder takes the concatenation of the base face generated in the first stage and the corresponding face landmark sketch as input and outputs a high-fidelity face through the guidance of the landmark sketch. The high-fidelity rendering process can be formulated as follows:

$$I^{HR} = \mathcal{F}^{HR}(I^B \oplus I^S), \quad (10)$$

where, \oplus indicate concatenation, I^S is the face landmark sketch, I^{HR} is the high-fidelity face, and \mathcal{F}^{HR} is the HRDecoder. We utilize the mediapipe tool [42] to detect the face landmark sketch from the base face. To optimize the HRDecoder, we use the model trained in the first stage to generate corresponding base faces and landmark sketches on the dataset as the training dataset for this stage.

2) *Loss Function for High-Fidelity Rendering:* To get high-fidelity faces, we define a discriminator, HRDiscriminator, at this stage. We use \mathcal{D}^{HR} to denote the HRDiscriminator. We train HRDiscriminator by adding the following loss:

$$\mathcal{L}_{disc}^{HR} = \mathbb{E}_{I^{GT}}[\log(1 - \mathcal{D}^{HR}(I^{GT}))] + \mathbb{E}_{I^{HR}}[\log(\mathcal{D}^{HR}(I^{HR}))], \quad (11)$$

HR Adversarial Loss: Same as Eq. 4, we employ adversarial loss to constrain the realism of HRDecoder:

$$\mathcal{L}_a^{HR} = \mathbb{E}_{I^{HR}}[\log(1 - \mathcal{D}^{HR}(I^{HR}))], \quad (12)$$

HR Perceptual Loss: We employ the pre-trained VGG [43], indicated as ϕ , to extract the image features and calculate the features l1 loss to constrain the generated images:

$$\mathcal{L}_p^{HR} = \frac{1}{N} \sum_{i=1}^N \|\phi(I^{HR}) - \phi(I^{GT})\|_1, \quad (13)$$

HR Reconstruction Loss: We also employ same as Eq. 5, constraining the l1 loss between the generated high-fidelity face and the GT:

$$\mathcal{L}_r^{HR} = \frac{1}{N} \sum_{i=1}^N \|I^{HR} - I^{GT}\|_1, \quad (14)$$

HR Lip Loss: To better optimize the lip region, we used the mask of the lip region to constrain the loss of lpiips and the reconstruction loss of the lip region.

$$\mathcal{L}_l^{HR} = \frac{1}{N} \sum_{i=1}^N (LPIPS(I_{lip}^{HR}, I_{lip}^{GT}) + \|(I^{HR} - I^{GT}) * I_{lip}^{mask}\|_1), \quad (15)$$

where I_{lip}^{HR} and I_{lip}^{GT} are the corped according to the lip bounding box of I^{HR} and I^{GT} , I_{lip}^{mask} is the lip mask.

The training loss for the high-fidelity rendering is:

$$\mathcal{L}_{total}^{HR} = \lambda_a^{HR} \mathcal{L}_a^{HR} + \lambda_p^{HR} \mathcal{L}_p^{HR} + \lambda_r^{HR} \mathcal{L}_r^{HR} + \lambda_l^{HR} \mathcal{L}_l^{HR}, \quad (16)$$

where λ_a^{HR} , λ_p^{HR} , λ_r^{HR} , λ_l^{HR} are the hyper-parameter weights.

IV. EXPERIMENTS

A. Experimental Settings

Implementation Details. We follow [8], [20] to process video frames with the centered crops of size 128×128 at 25 fps, and calculate Mel-spectrograms of size 16×80 from 16kHz audios using a window size of 800 and hop size of 200. For HyperLips-HR, we set the output upsampling to HR \times 1 by default, i.e. no upsampling, and the size of the output image remains at 128×128 . Hyper-parameters are empirically set: $\lambda_a^B=0.2$, $\lambda_r^B=0.5$, $\lambda_l^B=0.5$, $\lambda_{av}^B=0.3$, λ_a^{HR} , λ_p^{HR} , λ_r^{HR} , λ_l^{HR} are all set to 1. When training the HyperLips-Base and HyperLips-HR models, we set the learning rate to 0.0001 and used the Adam optimizer in PyTorch. All experiments are performed on a single NVIDIA TITAN RTX GPU.

TABLE I

QUANTITATIVE COMPARISON WITH STATE-OF-THE-ART TALKING FACE GENERATION METHODS ON LRS2 [41] DATASETS. \uparrow INDICATES HIGHER IS BETTER WHILE \downarrow INDICATES LOWER IS BETTER.

Method	PSNR \uparrow	SSIM \uparrow	LMD \downarrow	LSE-C \uparrow	LSE-D \downarrow
Wav2Lip [8]	31.794	0.894	1.471	6.841	7.202
ATVGnet [17]	32.812	0.871	1.984	4.610	8.445
SyncTalkFace [20]	32.138	0.886	1.354	4.725	8.368
IP_LAP [21]	33.281	0.891	1.494	3.435	9.398
HyperLips-Base(Ours)	33.953	0.914	1.186	6.707	6.878
HyperLips-HR(Ours)	34.914	0.820	1.203	5.939	7.504
Ground Truth	N/A	1.000	0.000	8.354	6.204

TABLE II

QUANTITATIVE COMPARISON WITH STATE-OF-THE-ART TALKING FACE GENERATION METHODS ON MEAD-NEUTRAL [45] DATASETS. \uparrow INDICATES HIGHER IS BETTER WHILE \downarrow INDICATES LOWER IS BETTER.

Method	PSNR \uparrow	SSIM \uparrow	LMD \downarrow	LSE-C \uparrow	LSE-D \downarrow
Wav2Lip [8]	29.867	0.683	2.294	2.312	10.488
DINet(O) [22]	30.056	0.707	2.367	1.710	11.560
DINet(R) [22]	28.573	0.621	1.838	1.203	11.906
IP_LAP [21]	30.578	0.699	1.386	1.349	11.868
HyperLips-Base(Ours)	30.784	0.721	1.294	1.266	11.854
HyperLips-HR(Ours)	31.503	0.747	1.237	1.271	11.861
Ground Truth	N/A	1.000	0.000	2.161	11.091

Dataset. Two audio-visual datasets, LRS2 [44] and MEAD-Neutral [45], are used in our experiments. **LRS2** is a sentence-level dataset with over 140,000 utterances, consists of 48,164 video clips from outdoor shows on BBC television. We randomly sample 80 videos from the test set for evaluating algorithms quantitatively. **MEAD-Neutral** is a part of MEAD dataset. MEAD dataset records around 40 hours emotional in-the-lab videos at 1080P resolution. We select a total of 1610 videos with neutral emotion and frontal view as MEAD-Neutral dataset and another 80 videos for testing.

Comparison Methods. We compare our method against state-of-the-art methods [8], [17], [20]–[22] on the person-generic audio-driven talking face generation. **Wav2Lip** [8] uses an encoder-decoder model learned via adversarial training to produce talking face videos. **ATVGnet** [17] takes advantage of 2D landmarks to generate talking face videos from the input audio and an identity frame. **SyncTalkFace** [20] proposes Audio-Lip Memory that brings in visual information of the mouth region corresponding to input audio and enforces fine-grained audio-visual coherence. **IP_LAP** [21] proposes a two-stage framework consisting of audio-to-landmark generation and landmark-to-video rendering procedures. **DINet** [22] proposes a Deformation Inpainting Network for high-resolution face visually dubbing. For more comparison settings, please refer to our supplementary document.

B. Evaluation Metrics

We use Peak Signal-to-Noise Ratio (**PSNR**) and Structured similarity (**SSIM**) [46] to measure the similarity between generated and ground-truth images. And we use dlib [47] to detect the lip landmark distances (**LMD**) between ground truth frames and those of generated frames. **LSE-C** and **LSE-D** proposed by [8] are cibfudebce score (higher the better)

and distance score (lower the better) between audio and video features from SyncNet [40], respectively. **LSE-C** and **LSE-D** measure correspondence between audio and visual features while **LMD** directly measures visual to visual coherence. For a fair comparison, we evaluate the cropped region of the face based on the face detector used in Wav2Lip [8].

We generate corresponding videos using different methods based on different audio in the test dataset. Specifically, the face in the video frame is first detected by face detection. Then, the corresponding face area is resized according to the required resolution size of the corresponding method. After the face is generated by the corresponding method, it is pasted back into the original video. For a fair comparison, frames extracted from talking face videos, which are cropped based on the face detector used in Wav2Lip are resized to 160×160 . When calculating the related metrics, we detect faces in the generated video and the corresponding ground truth video, resize them to 160×160 , and then perform frame-by-frame calculations. Wav2Lip synthesizes face with 96×96 resolution; DINet synthesizes face with 416×320 resolution; ATVGnet, IP_LAP, SyncTalkFace, and ours synthesize face with 128×128 resolution. For LSE-D and LSE-C, we generate talking face videos by inputting audio and face come from the different videos in test datasets and use SyncNet to calculate LSE-C and LSE-D with generating talking face videos.

C. Quantitative Comparison

Table I and II show the quantitative comparison on the LRS2 and MEAD-Neutral datasets, respectively. DINet(O) indicates tested on the MEAD dataset using the checkpoints officially released by DINet. DINet(R) is the result of our reproduction on the MEAD-Neutral dataset according to the code of DINet. In the tables, our HyperLips-HR output resolution is 128×128 without upsampling. The results show that whether it is our HyperLips-Base or our HyperLips-HR, the generated faces are significantly better than other methods in terms of PSNR, SSIM, and LMD metrics. Our HyperLips-HR is significantly better than our HyperLips-Base in terms of PSNR and SSIM, which shows that our HRDecoder has enhanced high-fidelity face rendering. However, there is no significant increase in the LMD metric, which shows that HRDecoder does not help improve lip synchronization. Regarding PSNR and SSIM, our results in Table 1 are better than those in Table 2. This is because the face quality in the LRS2 dataset is worse than that in the MEAD dataset, making it easier for the faces generated by our model to reach the quality of LRS2.

For LSE-C and LSE-D, Wav2Lip perform better results and even outperforms those of ground truth. The weights ¹ of SyncNet we used in the test were derived from [40] without fine-tuning. In fact, these two metrics have been discussed in [20], [48], it only proves that their lip-sync results are nearly comparable to the ground truth, not better. On the one hand, the dataset used for model training may not match the

¹SyncNet Weights: http://www.robots.ox.ac.uk/vgg/software/lipsync/data/syncnet_v2.model

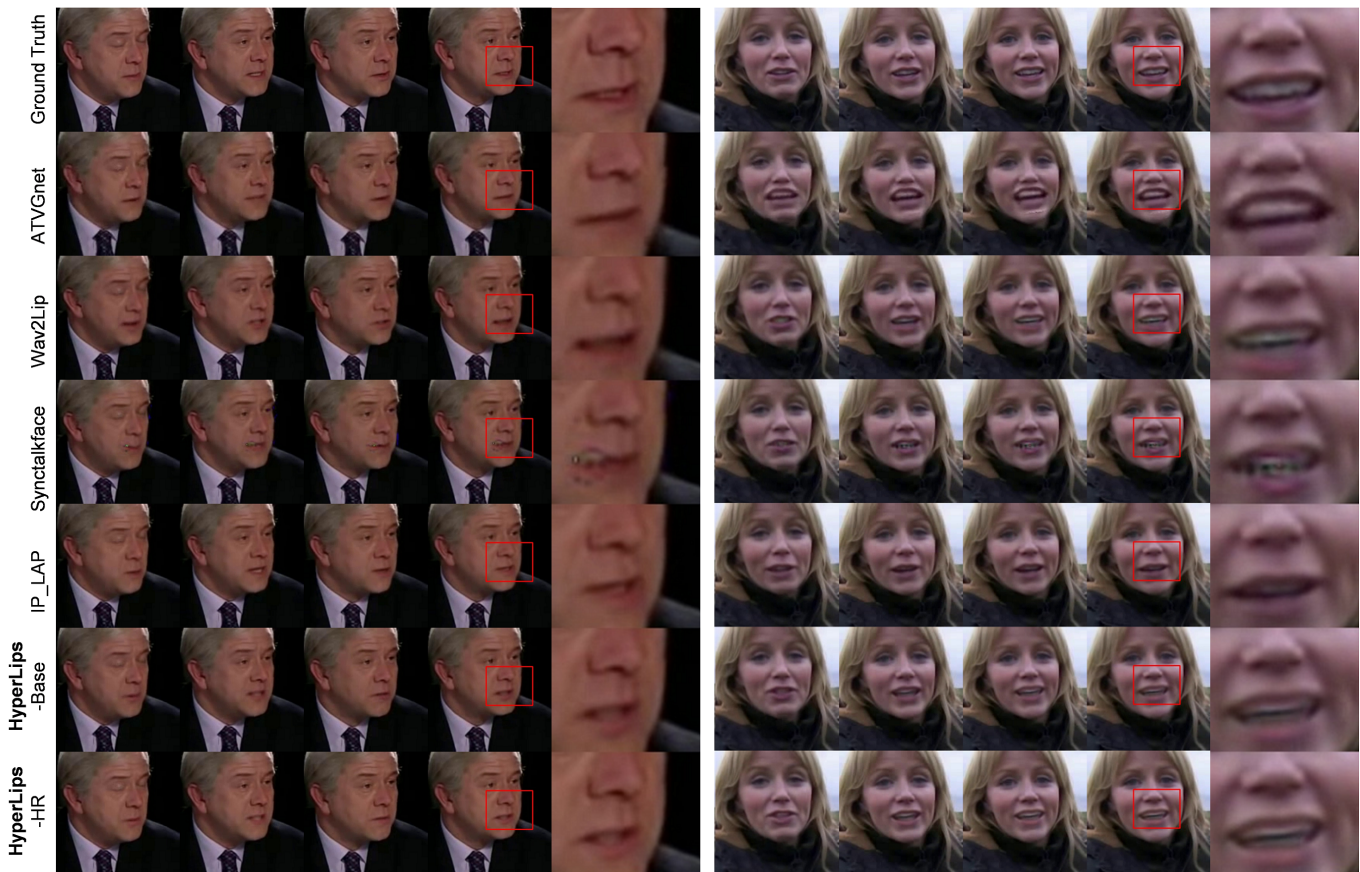


Fig. 3. Qualitative comparisons with state-of-the-art methods on LRS2 datasets. Our method is capable of rendering more high-fidelity faces. More results are presented in the supplementary material.

distribution of the dataset we tested, resulting in two test results that may not accurately reflect lip synchronization; on the other hand, we performed better on the LMD metric, which is another synchronization metric that measures correspondence in the visual domain.

D. Qualitative Comparison

User Study. To verify the video quality and lip synchronization of our talking face generation method, we invited 20 participants to evaluate the generated videos. We randomly selected 5 videos from the MEAD-Neutral [45] test dataset and generated different videos using different methods: Wav2Lip [8], IP_LAP [21], DInet(R) [22], DInet(O) [22] and HyperLips-HR(Ours). We asked the participants to vote for the video in two evaluation indicators: video quality of the results and whether to keep the lip synchronization. We collected 100 votes for each evaluation indicator and presented the result as a box plot in Fig. 5. As can be seen, our results stand out from other methods in terms of video quality and lip synchronization.

Visualization Comparison. Fig. 3 and Fig. 4 show examples from LRS2 and MEAD-Neural dataset, respectively. Compared to other methods, our method produces images that are visually closer to the ground truth and show no artifacts in our results. The superiority of our method cannot be seen on the LRS2 dataset because the faces in this dataset are relatively blurred. But on the MEAD dataset, our method produces

TABLE III
ABLATION STUDY ON THE SIZE OF HRDECODER OUTPUT.

Dataset	Size	PSNR \uparrow	SSIM \uparrow	LMD \downarrow	LSE-C \uparrow	LSE-D \downarrow
LRS2	S=128(Base)	33.953	0.914	1.186	6.707	6.878
	S=128(HR \times 1)	34.914	0.920	1.203	5.939	7.504
	S=256(HR \times 2)	35.159	0.924	1.070	4.965	8.400
	S=512(HR \times 4)	34.895	0.921	1.175	5.580	7.835
MEAD-Neural	S=128(Base)	30.784	0.721	1.294	1.266	11.854
	S=128(HR \times 1)	31.503	0.747	1.237	1.271	11.861
	S=256(HR \times 2)	31.539	0.747	1.204	1.265	11.863
	S=512(HR \times 4)	31.460	0.750	1.210	1.255	11.879

results that render faces clearly, and even teeth can be seen clearly. Our method also excels in lip sync. For example, in the last face on the left in Fig. 4, our results perfectly reproduce the current mouth shape, which is slightly open with teeth exposed, but the results from IP_LAP are not.

E. Ablation Study

In this section, we perform ablation studies to validate the effect of core components in our method and the performance gain derived from high-fidelity rendering.

The Size of HRDecoder Output. Our input in the high-fidelity rendering stage is fixed at 128×128 , and the output can render faces with different resolutions, such as 128×128 (HR \times 1), 256×256 (HR \times 2), and 512×512 (HR \times 4), through the transposed convolution of HRDecoder. High-resolution

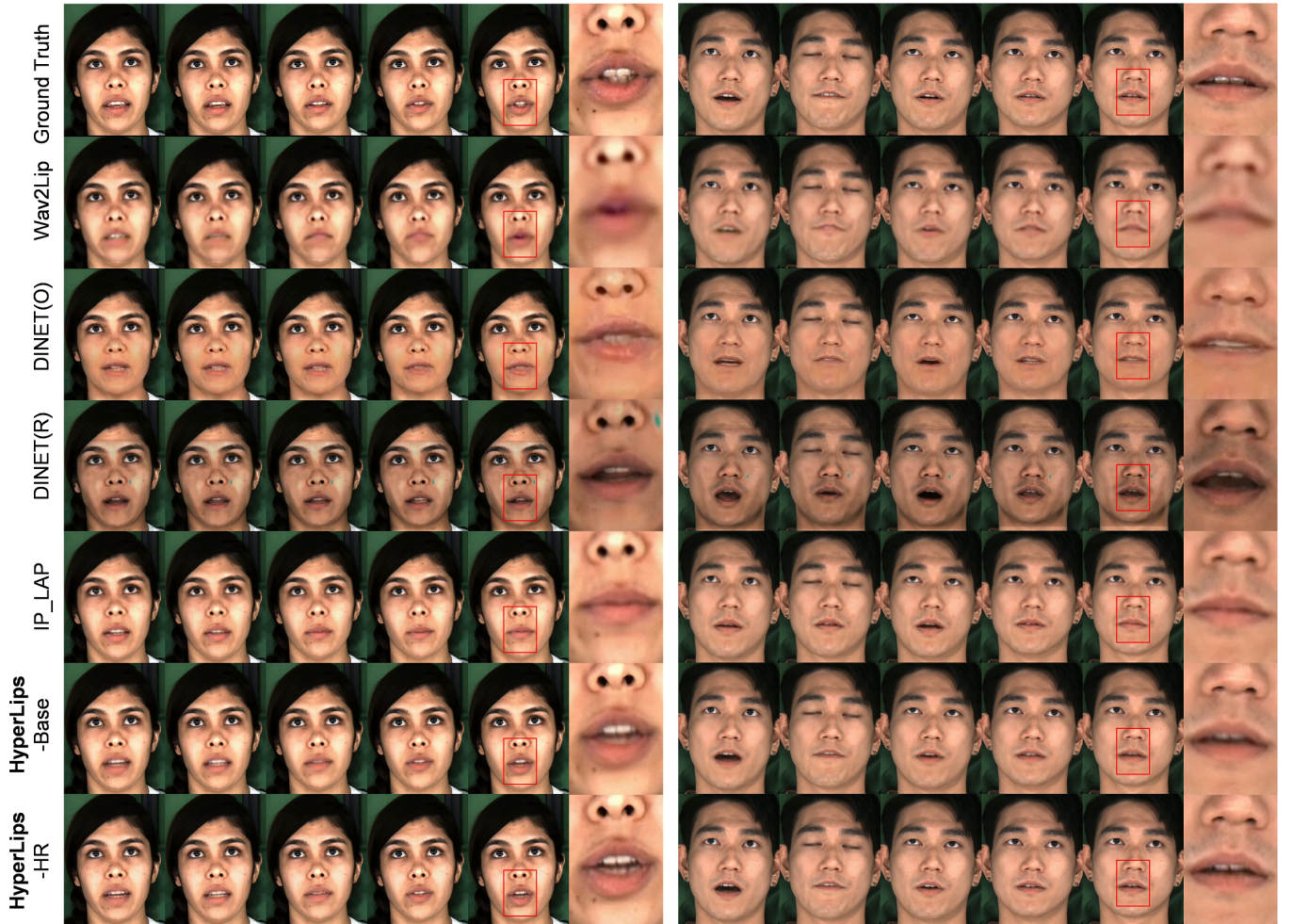


Fig. 4. Qualitative comparisons with state-of-the-art methods on MEAD-Neutral datasets. Our method is capable of rendering more high-fidelity faces. More results are presented in the supplementary material.

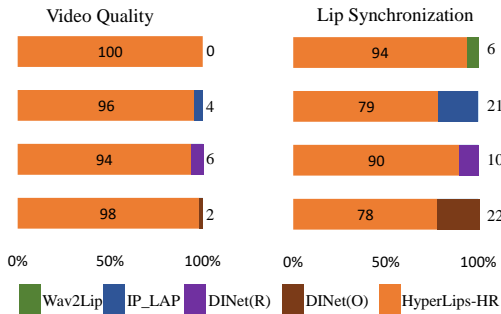


Fig. 5. User study about video quality and lip synchronization.

TABLE IV
ABLATION STUDY ON EFFECTIVENESS FOR SKETCH INPUT OF HRDECODER.

Method	PSNR \uparrow	SSIM \uparrow	LMD \downarrow	LSE-C \uparrow	LSE-D \downarrow
Base	30.784	0.721	1.294	1.266	11.854
HR \times 1(w/o sketch)	30.762	0.727	1.305	1.244	11.938
HR \times 1(w/ sketch)	31.503	0.747	1.237	1.271	11.861
HR \times 2(w/o sketch)	30.543	0.734	1.300	1.225	11.853
HR \times 2(w/ sketch)	31.539	0.747	1.204	1.265	11.863
HR \times 4(w/o sketch)	30.281	0.730	1.348	1.216	12.004
HR \times 4(w/ sketch)	31.460	0.750	1.210	1.255	11.879

TABLE V
ABLATION STUDY ON EFFECTIVENESS FOR FINETUNING.

Method	PSNR \uparrow	SSIM \uparrow	LMD \downarrow	LSE-C \uparrow	LSE-D \downarrow
Base(w/o fineturn, MEAD)	31.200	0.834	1.259	3.050	10.463
Base(w/ fineturn, MEAD)	31.672	0.850	1.199	3.210	10.527
HR(w/ fineturn, MEAD)	31.917	0.842	1.164	3.594	10.239
Base(w/o fineturn, LRS2)	31.303	0.826	1.150	4.054	9.587
Base(w/ fineturn, LRS2)	31.846	0.851	1.164	3.516	10.565
HR(w/ fineturn, LRS2)	32.012	0.845	1.164	3.516	10.261
GT	N/A	1.000	0.000	3.615	10.309

faces can often produce finer images, which are convenient for application to high-resolution videos. In Table III, we study the effect of different output sizes on the LRS2 and MEAD datasets. Our HR models significantly compares with the Base model regarding image quality (such as PSNR and SSIM metrics), e.g., PSNR, the HR \times 1 model is 34.914, and the Base model is 33.953. However, in terms of lip synchronization (such as LMD indicators), the HR models are only comparable to the Base model. However, for all HR models, the image quality index does not increase significantly with increasing size, and even the image quality at size 512×512 is comparable to that at size 128×128 . It can be concluded that on the LRS2 and MEAD datasets, a size of 256×256

can already provide a cost-effective result.

Effectiveness for Sketch Input of HRDecoder. In HRDecoder, we introduced face landmark sketches to guide the generation of high-fidelity face images. We performed corresponding ablation experiments on the MEAD dataset to verify the influence of sketches as input to HRDecoder on the rendering results. In Table IV, “w/o sketch” means that no face landmark sketches are used as input, and “w/ sketch” means that face landmark sketches are used as input. The results show that in all HR models, the rendering results of adding face landmark sketches as a guide input are better than the rendering results without adding sketches. This suggests that sketches are beneficial for generating high-fidelity face images.

Effectiveness for Finetuning. Although our method supports dubbing any face video, it may generally perform poorly on unseen faces. Therefore, we performed an ablation experiment on this. We chose a video of Kate’s speech and used 4 minutes and 40 seconds of the video as training data and another 18 seconds as test data. As shown in Table V, we fine-tuned the pre-trained models on the MEAD and LRS2 datasets to Kate’s videos and obtained corresponding results. The results show that the deformed model produces slightly better results in terms of visual quality without a significant improvement in lip synchronization.



Fig. 6. The Impact of Landmark Detection Failure

The Impact of Landmark Detection Failure. There is a defect in landmark-based talking face generation methods (such as IP_LAP, ATVGnet, etc.). That is, faces cannot be generated if landmark detection fails. There is no such problem with those that are not based on landmark detection, such as Wav2Lip, etc. Our method is not based on landmark detection in the first stage (Base model), so it can still generate the correct face even if the face deviation is severe, as shown in Fig. 6. As for the second stage (HR models), our method still has such shortcomings.

V. CONCLUSION

We propose a hypernetwork for controlling lip movements with audio information to achieve lip synchronization in the task of talking face generation. We first use a FaceEncoder to extract the visual face information as latent code from the source video; and then use HyperConv to modify the latent code to synchronize the lip movement with the audio; finally, FaceDecoder will decode the modified and synchronized latent

code into visual face content. The weight parameters are updated by HyperNet using the audio features as input. In order to achieve high-fidelity human face rendering, we propose HRDecoder, which uses landmark guidance as the face detail enhancement of faces. Therefore, our method effectively improves lip synchronization and face visual quality.

REFERENCES

- [1] M. Toshpulatov, W. Lee, and S. Lee, “Talking human face generation: A survey,” *Expert Systems with Applications*, p. 119678, 2023.
- [2] Y. Chen, B. Guo, Y. Shen, W. Wang, W. Lu, and X. Suo, “Boundary graph convolutional network for temporal action detection,” *Image and Vision Computing*, vol. 109, p. 104144, 2021.
- [3] —, “Capsule boundary network with 3d convolutional dynamic routing for temporal action detection,” *IEEE Transactions on Circuits and Systems for Video Technology*, vol. 32, no. 5, pp. 2962–2975, 2021.
- [4] Y. Chen, B. Guo, Y. Shen, R. Zhou, W. Lu, W. Wang, X. Wen, and X. Suo, “Video summarization with u-shaped transformer,” *Applied Intelligence*, vol. 52, no. 15, pp. 17 864–17 880, 2022.
- [5] L. Xie and Z.-Q. Liu, “Realistic mouth-synching for speech-driven talking face using articulatory modelling,” *IEEE Transactions on Multimedia*, vol. 9, no. 3, pp. 500–510, 2007.
- [6] L. Yu, H. Xie, and Y. Zhang, “Multimodal learning for temporally coherent talking face generation with articulator synergy,” *IEEE Transactions on Multimedia*, vol. 24, pp. 2950–2962, 2021.
- [7] P. KR, R. Mukhopadhyay, J. Philip, A. Jha, V. Namboodiri, and C. Jawahar, “Towards automatic face-to-face translation,” in *Proceedings of the 27th ACM international conference on multimedia*, 2019, pp. 1428–1436.
- [8] K. Prajwal, R. Mukhopadhyay, V. P. Namboodiri, and C. Jawahar, “A lip sync expert is all you need for speech to lip generation in the wild,” in *Proceedings of the 28th ACM International Conference on Multimedia*, 2020, pp. 484–492.
- [9] T. Xie, L. Liao, C. Bi, B. Tang, X. Yin, J. Yang, M. Wang, J. Yao, Y. Zhang, and Z. Ma, “Towards realistic visual dubbing with heterogeneous sources,” in *Proceedings of the 29th ACM International Conference on Multimedia*, 2021, pp. 1739–1747.
- [10] J. Thies, M. Elgharib, A. Tewari, C. Theobalt, and M. Nießner, “Neural voice puppetry: Audio-driven facial reenactment,” in *European conference on computer vision*. Springer, 2020, pp. 716–731.
- [11] S. Ravichandran, O. Texler, D. Dinev, and H. J. Kang, “Synthesizing photorealistic virtual humans through cross-modal disentanglement,” in *Proceedings of the IEEE/CVF Conference on Computer Vision and Pattern Recognition*, 2023, pp. 4585–4594.
- [12] J. Tang, K. Wang, H. Zhou, X. Chen, D. He, T. Hu, J. Liu, G. Zeng, and J. Wang, “Real-time neural radiance talking portrait synthesis via audio-spatial decomposition,” *arXiv preprint arXiv:2211.12368*, 2022.
- [13] Y. Guo, K. Chen, S. Liang, Y.-J. Liu, H. Bao, and J. Zhang, “Adnerf: Audio driven neural radiance fields for talking head synthesis,” in *Proceedings of the IEEE/CVF International Conference on Computer Vision*, 2021, pp. 5784–5794.
- [14] Z. Ye, Z. Jiang, Y. Ren, J. Liu, J. He, and Z. Zhao, “Geneface: Generalized and high-fidelity audio-driven 3d talking face synthesis,” *arXiv preprint arXiv:2301.13430*, 2023.
- [15] Z. Ye, J. He, Z. Jiang, R. Huang, J. Huang, J. Liu, Y. Ren, X. Yin, Z. Ma, and Z. Zhao, “Geneface++: Generalized and stable real-time audio-driven 3d talking face generation,” *arXiv preprint arXiv:2305.00787*, 2023.
- [16] A. Chatziagapi, S. Athar, A. Jain, M. Rohith, V. Bhat, and D. Samaras, “Lipnerf: What is the right feature space to lip-sync a nerf?” in *2023 IEEE 17th International Conference on Automatic Face and Gesture Recognition (FG)*. IEEE, 2023, pp. 1–8.
- [17] L. Chen, R. K. Maddox, Z. Duan, and C. Xu, “Hierarchical cross-modal talking face generation with dynamic pixel-wise loss,” in *Proceedings of the IEEE/CVF conference on computer vision and pattern recognition*, 2019, pp. 7832–7841.
- [18] W. Zhang, X. Cun, X. Wang, Y. Zhang, X. Shen, Y. Guo, Y. Shan, and F. Wang, “Sadtalker: Learning realistic 3d motion coefficients for stylized audio-driven single image talking face animation,” in *Proceedings of the IEEE/CVF Conference on Computer Vision and Pattern Recognition*, 2023, pp. 8652–8661.
- [19] S. E. Eskimez, Y. Zhang, and Z. Duan, “Speech driven talking face generation from a single image and an emotion condition,” *IEEE Transactions on Multimedia*, vol. 24, pp. 3480–3490, 2021.

- [20] S. J. Park, M. Kim, J. Hong, J. Choi, and Y. M. Ro, "Synctalkface: Talking face generation with precise lip-syncing via audio-lip memory," in *Proceedings of the AAAI Conference on Artificial Intelligence*, vol. 36, no. 2, 2022, pp. 2062–2070.
- [21] W. Zhong, C. Fang, Y. Cai, P. Wei, G. Zhao, L. Lin, and G. Li, "Identity-preserving talking face generation with landmark and appearance priors," in *Proceedings of the IEEE/CVF Conference on Computer Vision and Pattern Recognition*, 2023, pp. 9729–9738.
- [22] Z. Zhang, Z. Hu, W. Deng, C. Fan, T. Lv, and Y. Ding, "Dinet: Deformation inpainting network for realistic face visually dubbing on high resolution video," 2023.
- [23] Z. Ye, M. Xia, R. Yi, J. Zhang, Y.-K. Lai, X. Huang, G. Zhang, and Y.-j. Liu, "Audio-driven talking face video generation with dynamic convolution kernels," *IEEE Transactions on Multimedia*, 2022.
- [24] D. Bigioi, S. Basak, H. Jordan, R. McDonnell, and P. Corcoran, "Speech driven video editing via an audio-conditioned diffusion model," *arXiv preprint arXiv:2301.04474*, 2023.
- [25] B. Mildenhall, P. P. Srinivasan, M. Tancik, J. T. Barron, R. Ramamoorthi, and R. Ng, "Nerf: Representing scenes as neural radiance fields for view synthesis," *Communications of the ACM*, vol. 65, no. 1, pp. 99–106, 2021.
- [26] D. Ha, A. Dai, and Q. V. Le, "Hypernetworks," in *ICLR*, 2017.
- [27] P.-Z. Chiang, M.-S. Tsai, H.-Y. Tseng, W.-S. Lai, and W.-C. Chiu, "Stylizing 3d scene via implicit representation and hypernetwork," in *Proceedings of the IEEE/CVF Winter Conference on Applications of Computer Vision*, 2022, pp. 1475–1484.
- [28] Y. Chen, Q. Yuan, Z. Li, C. Xie, Y. Liu, W. Wang, X. Wen, and Q. Yu, "Upst-nerf: Universal photorealistic style transfer of neural radiance fields for 3d scene," *arXiv preprint arXiv:2208.07059*, 2022.
- [29] A. Radford, K. Narasimhan, T. Salimans, I. Sutskever *et al.*, "Improving language understanding by generative pre-training," 2018.
- [30] A. Radford, J. Wu, R. Child, D. Luan, D. Amodei, I. Sutskever *et al.*, "Language models are unsupervised multitask learners," *OpenAI blog*, vol. 1, no. 8, p. 9, 2019.
- [31] T. Brown, B. Mann, N. Ryder, M. Subbiah, J. D. Kaplan, P. Dhariwal, A. Neelakantan, P. Shyam, G. Sastry, A. Askell *et al.*, "Language models are few-shot learners," *Advances in neural information processing systems*, vol. 33, pp. 1877–1901, 2020.
- [32] B. Peng, C. Li, P. He, M. Galley, and J. Gao, "Instruction tuning with gpt-4," *arXiv preprint arXiv:2304.03277*, 2023.
- [33] R. Rombach, A. Blattmann, D. Lorenz, P. Esser, and B. Ommer, "High-resolution image synthesis with latent diffusion models," in *Proceedings of the IEEE/CVF conference on computer vision and pattern recognition*, 2022, pp. 10 684–10 695.
- [34] A. Q. Wang, A. V. Dalca, and M. R. Sabuncu, "Regularization-agnostic compressed sensing mri reconstruction with hypernetworks," *arXiv preprint arXiv:2101.02194*, 2021.
- [35] T. Wang, K. Zhang, X. Chen, W. Luo, J. Deng, T. Lu, X. Cao, W. Liu, H. Li, and S. Zafeiriou, "A survey of deep face restoration: Denoise, super-resolution, deblur, artifact removal," *arXiv preprint arXiv:2211.02831*, 2022.
- [36] Y. Chen, Y. Tai, X. Liu, C. Shen, and J. Yang, "Fsrnet: End-to-end learning face super-resolution with facial priors," in *Proceedings of the IEEE conference on computer vision and pattern recognition*, 2018, pp. 2492–2501.
- [37] Z. Shen, W.-S. Lai, T. Xu, J. Kautz, and M.-H. Yang, "Deep semantic face deblurring," in *Proceedings of the IEEE conference on computer vision and pattern recognition*, 2018, pp. 8260–8269.
- [38] Y. Yin, J. Robinson, Y. Zhang, and Y. Fu, "Joint super-resolution and alignment of tiny faces," in *Proceedings of the AAAI Conference on Artificial Intelligence*, vol. 34, no. 07, 2020, pp. 12 693–12 700.
- [39] R. Zhang, P. Isola, A. A. Efros, E. Shechtman, and O. Wang, "The unreasonable effectiveness of deep features as a perceptual metric," in *Proceedings of the IEEE conference on computer vision and pattern recognition*, 2018, pp. 586–595.
- [40] J. S. Chung and A. Zisserman, "Out of time: automated lip sync in the wild," in *Asian conference on computer vision*. Springer, 2016, pp. 251–263.
- [41] T. Afouras, J. S. Chung, A. Senior, O. Vinyals, and A. Zisserman, "Deep audio-visual speech recognition," *IEEE transactions on pattern analysis and machine intelligence*, vol. 44, no. 12, pp. 8717–8727, 2018.
- [42] C. Lugaresi, J. Tang, H. Nash, C. McClanahan, E. Uboweja, M. Hays, F. Zhang, C.-L. Chang, M. G. Yong, J. Lee *et al.*, "Mediapipe: A framework for building perception pipelines," *arXiv preprint arXiv:1906.08172*, 2019.
- [43] K. Simonyan and A. Zisserman, "Very deep convolutional networks for large-scale image recognition," *arXiv preprint arXiv:1409.1556*, 2014.
- [44] T. Afouras, J. S. Chung, A. Senior, O. Vinyals, and A. Zisserman, "Deep audio-visual speech recognition," in *arXiv:1809.02108*, 2018.
- [45] K. Wang, Q. Wu, L. Song, Z. Yang, W. Wu, C. Qian, R. He, Y. Qiao, and C. C. Loy, "Mead: A large-scale audio-visual dataset for emotional talking-face generation," in *European Conference on Computer Vision*. Springer, 2020, pp. 700–717.
- [46] Z. Wang, A. C. Bovik, H. R. Sheikh, and E. P. Simoncelli, "Image quality assessment: from error visibility to structural similarity," *IEEE transactions on image processing*, vol. 13, no. 4, pp. 600–612, 2004.
- [47] D. E. King, "Dlib-ml: A machine learning toolkit," *The Journal of Machine Learning Research*, vol. 10, pp. 1755–1758, 2009.
- [48] H. Zhou, Y. Sun, W. Wu, C. C. Loy, X. Wang, and Z. Liu, "Pose-controllable talking face generation by implicitly modularized audio-visual representation," in *Proceedings of the IEEE/CVF conference on computer vision and pattern recognition*, 2021, pp. 4176–4186.
- [49] X. Wang, Y. Li, H. Zhang, and Y. Shan, "Towards real-world blind face restoration with generative facial prior," in *Proceedings of the IEEE/CVF conference on computer vision and pattern recognition*, 2021, pp. 9168–9178.

VI. SUPPLEMENTARY MATERIAL

A. Post Processing

Generated Face Fusion: In order to obtain a more natural driving effect, we followed [21] to create a post-processing process. As shown in Fig. 7, *Predicted* is the face image predicted by our model, denote as I^P ; *Face Mask* is the face mask parsed from the predicted face image using the Face Parsing method, denote as α ; *Reference* is the reference face image, denote as I^R ; *Background Mask* is equal to $(I - \alpha)$; the *Fine Result* can be formulated as follows:

$$I^{fine} = I^P \times \alpha + I^R \times (1 - \alpha), \quad (17)$$

We take the generated face image out of the eyebrows, eyes and nose, and paste the rest back to the reference image.

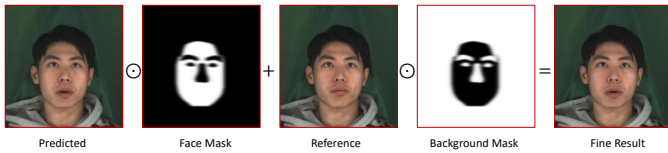


Fig. 7. Post Processing for Generated Face Fusion.

Face Enhancement: Even though our method can produce a high-fidelity face with clear lips, in the actual production process, it may still not be perfect in the following cases: 1. The reference video (source video) is blurred; 2. Not performed better fine-tuning training. The face restoration algorithm can further improve the quality of the generated faces. Fig. 8 shows the enhanced effect of the face restoration algorithm: We drive the reference video with hyperlips to get the lip-sync generated video, and then use GFP-GAN [49] to enhance the generated video. It can be seen that the enhanced video is clearer in facial details. But this method also has obvious disadvantages, that is, after the face is enhanced, there will be artifacts in the enhanced face due to the GAN technology, and there will be a certain deviation from the real original face.

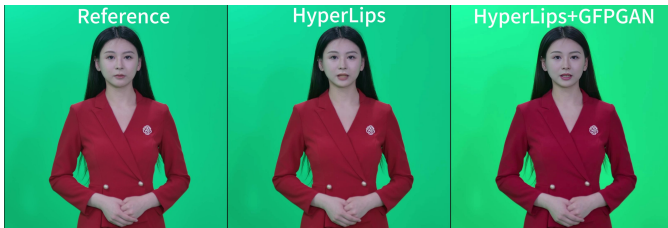
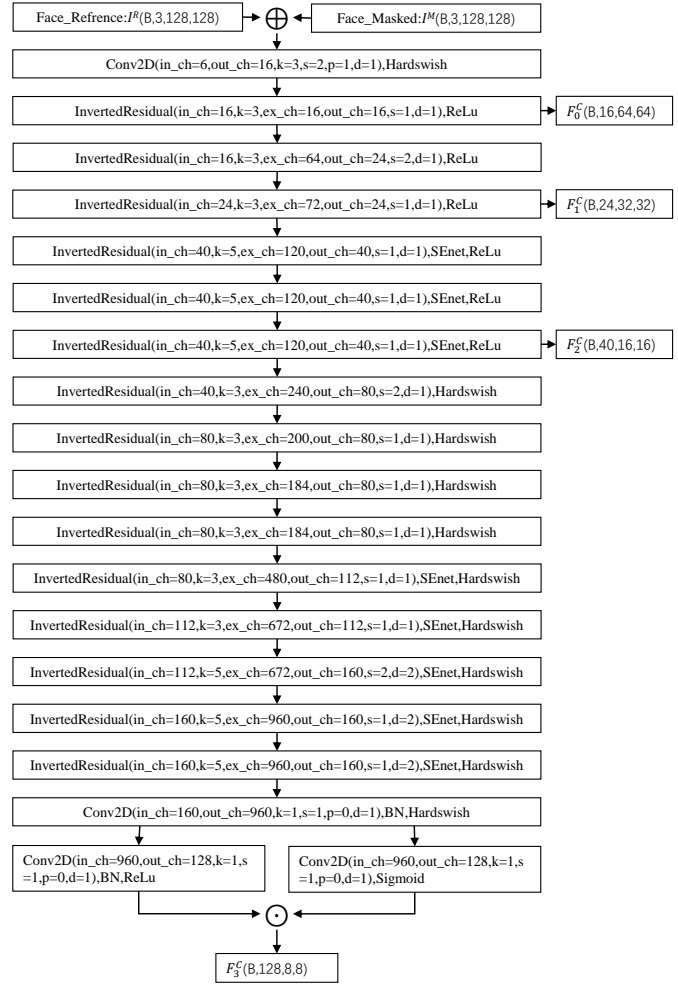


Fig. 8. Post Processing for Face Enhancement.

B. Configuration of HyperLips Model

Our proposed model has been divided into two stages: Base Face Generation and High-Fidelity Rendering. Here, we list the configuration of each sub-module included in the two stages in detail


 Fig. 9. Configuration of FaceEncoder. \oplus indicate concatenation, \otimes indicate multiplication, in_ch indicate the number of input channel, out_ch indicate the number of out channel, ex_ch indicate the number of extension channel, k indicate the kernel size, s indicate the stride size, p indicate the padding size.

In the Base Face Generation stage, it includes FaceEncoder, AudioEncoder, FaceDecoder, HyperNet, and HyperConv sub-modules. The detailed configuration of these sub-modules is shown in Fig. 9, 10, 11, 12, and 13 respectively. For FaceEncoder and AudioEncoder, the network architecture is the same, but the input feature size is not the same, therefore, the output feature size is also different. For FaceEncoder, the input is the concatenation of Reference and Masked, therefore, the input size is $B \times 6 \times 128 \times 128$; For AudioEncoder, the input is Mel-spectrogram of the audio, and the size is $B \times 1 \times 80 \times 60$, where B indicate the batch size.

In the High-Fidelity Rendering stage, only one module, HRDecoder, consists of three parts: conv_base, up_conv and out_put_block. Although HRDecoder is relatively simple, it has three variants that allow the model to render face images of different resolutions: $HR \times 1$, the configuration shows in Fig. 14, and the output image size is 128×128 ; $HR \times 2$, the configuration shows in Fig. 15, and the output image size is 256×256 ; $HR \times 4$, the configuration shows in Fig. 16, and the

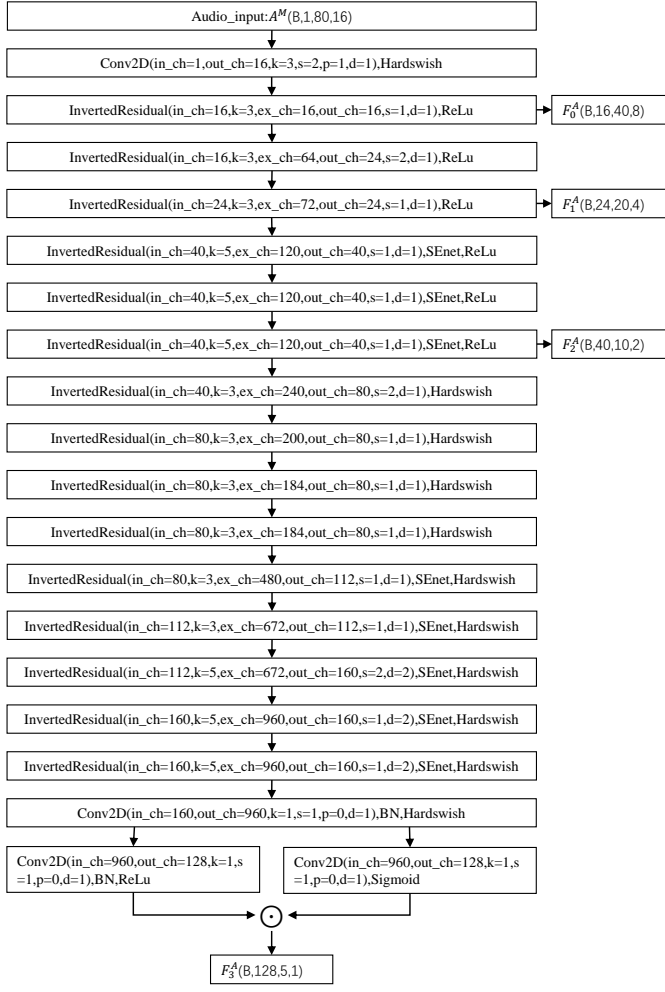


Fig. 10. Configuration of AudioEncoder. \oplus indicate concatenation, \odot indicate multiplication, in_ch indicate the number of input channel, out_ch indicate the number of out channel, ex_ch indicate the number of extension channel, k indicate the kernel size, s indicate the stride size, p indicate the padding size.

output image size is 512×512 . The input to HRDecoder is the concatenation feature of the base face with the sketch extracted from the base face, and the output is the high-fidelity face. We use Transpose Convolution to realize the conversion of feature maps from low resolution to high resolution. In $HR \times 1$, we did not use transpose convolution, so the output size is the same as the input; in $HR \times 2$, we use one transpose convolution, so the output size is twice the input; in $HR \times 4$, we use two transpose convolution, so the output size is four times the input.

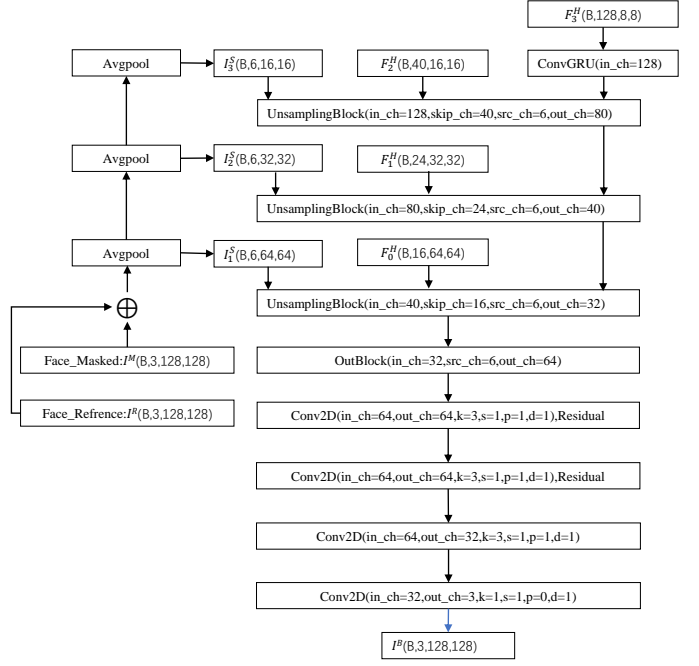


Fig. 11. Configuration of FaceDecoder. \oplus indicate concatenation, in_ch indicate the number of input channel, out_ch indicate the number of out channel, k indicate the kernel size, s indicate the stride size, p indicate the padding size.

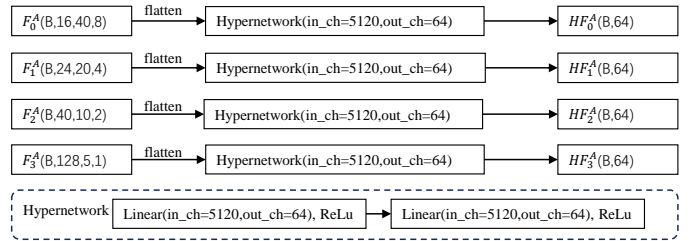


Fig. 12. Configuration of HyperNet.

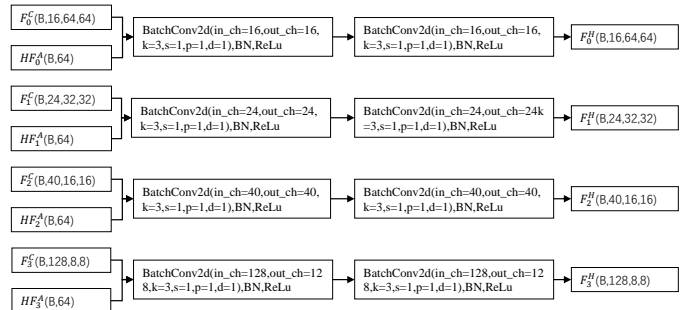


Fig. 13. Configuration of HyperConv. in_ch indicate the number of input channel, out_ch indicate the number of out channel, k indicate the kernel size, s indicate the stride size, p indicate the padding size.

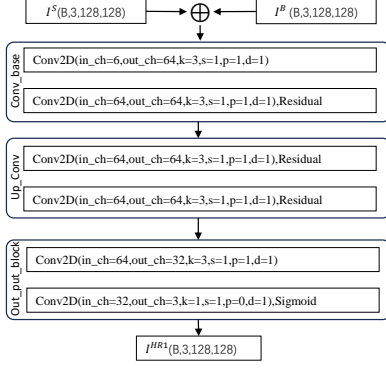


Fig. 14. Configuration of $HR \times 1$. \oplus indicate concatenation, in_ch indicate the number of input channel, out_ch indicate the number of out channel, k indicate the kernel size, s indicate the stride size, p indicate the padding size.

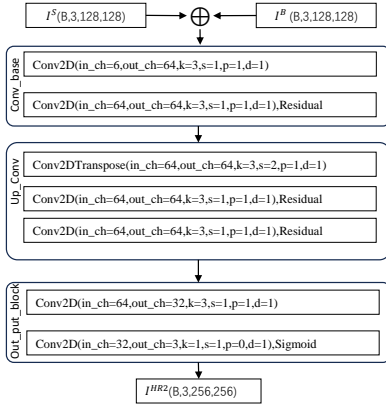


Fig. 15. Configuration of $HR \times 2$. \oplus indicate concatenation, in_ch indicate the number of input channel, out_ch indicate the number of out channel, k indicate the kernel size, s indicate the stride size, p indicate the padding size.

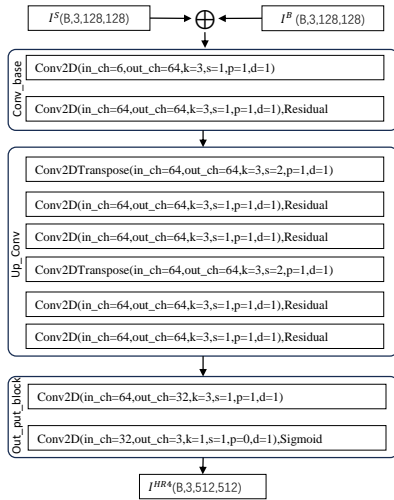


Fig. 16. Configuration of $HR \times 4$. \oplus indicate concatenation, in_ch indicate the number of input channel, out_ch indicate the number of out channel, k indicate the kernel size, s indicate the stride size, p indicate the padding size.

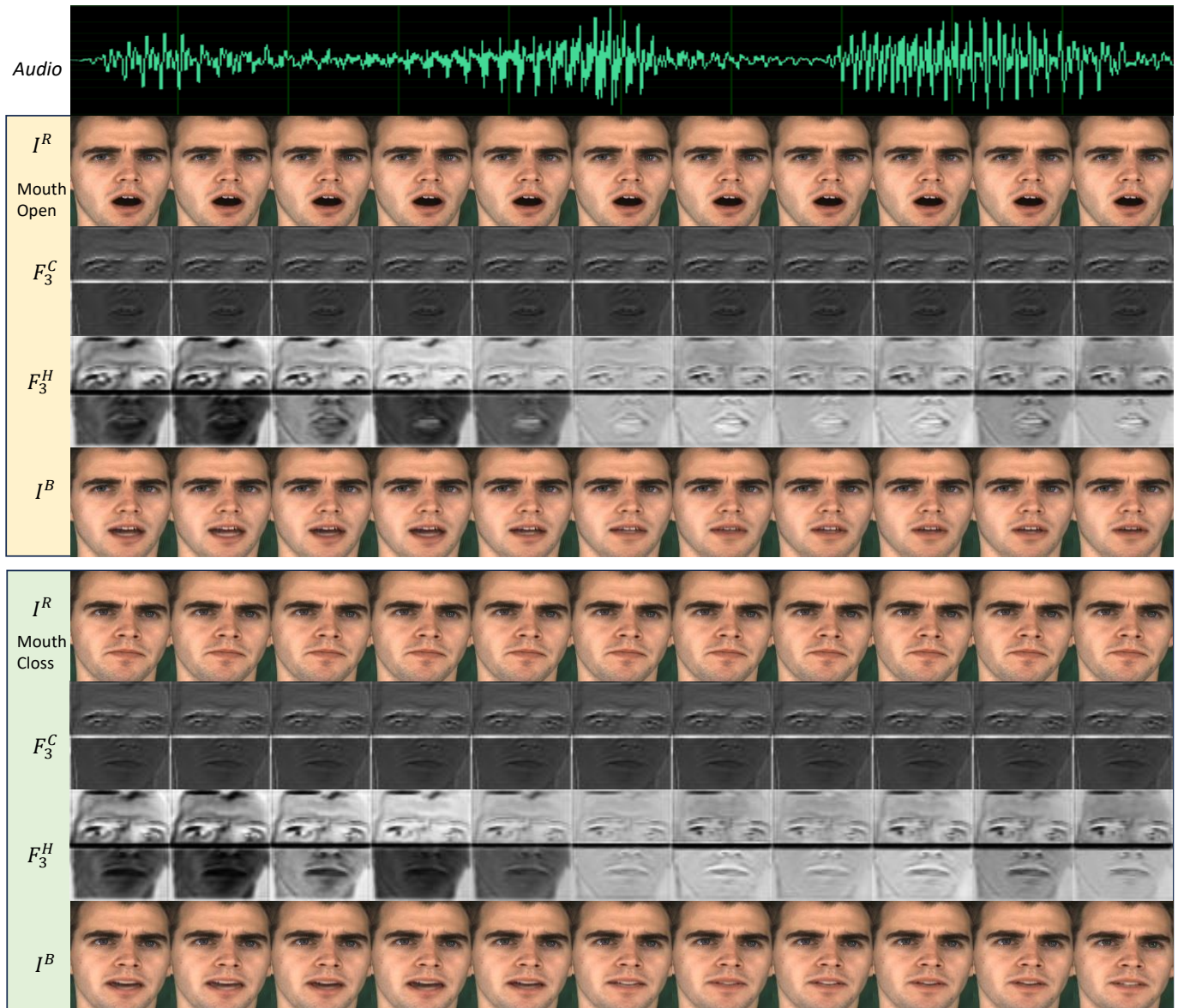


Fig. 17. Effect of Reference Video on Results.

C. Effect of Reference Video on Results

The reference video carries the identity information of the driven character, which directly affects the character influence of the generated video. The expressions, poses, movements, and other information of the characters in the generated video are also directly obtained from the reference video. Therefore, the videos generated by our method naturally have more natural expressions, postures, and movements of the characters.

However, in addition to the above effects, the mouth shape of the reference video also has a greater effects on the mouth shape of the generated video, as shown in Fig. 17, which we study in detail. We choose a fixed frame as the input for the whole reference video I^R . The mouth of the person in the reference video in the yellow part is open, while the mouth of the person in the reference video in the green part is closed. We

can see that at the same moment, the mouth of the I^B obtained by using the open mouth as the reference video input is larger than the mouth of the I^B obtained by using the closed mouth as the reference input. This phenomenon can also be seen in the I_3^H feature map in FaceDecoder. This is because the mouth shape state of the input reference video remains the same state after FaceEncoder (see I_3^C). Therefore, it is not difficult to conclude that if the mouth in the reference video moves (i.e., talking) with timing and is inconsistent with the driving audio, it may cause the generated lips to be less lip-synchronous or cause lip-smacking. Based on the above conclusions, if we want to get a better driving performance, we should choose a video in which the mouth does not move as a reference video. If it is expected that the mouth of the person in the generated video will be wider, the mouth of the selected reference video must be kept wider.

D. Additional Visualization Comparison

Visualization of Effectiveness for Finetuning. In our paper, we show the fine-tuned the pre-trained models on the MEAD and LRS2 datasets to Kate's videos and obtained corresponding results. Here, in Fig. 18, we show the Visualization of Effectiveness for Finetuning. The results obtained by fine-tuning the pre-trained model on the data set of higher quality (e.g., MEAD-Neutral [45]) are better and clearer than the results obtained by fine-tuning the pre-trained model on the data set of lower quality (e.g., LRS2 [41]).

Visualization Comparison with State-of-the-art: We show more visualization comparisons on the LRS2 and MEAD datasets in Fig. 19, Fig. 20, Fig. 21, Fig. 22, etc. These comparisons include our base model as well as all HR models. The results show that our method outperforms in terms of visual quality and lip synchronization. This excellence is more evident on high-definition datasets (such as the MEAD dataset).



Fig. 18. Visualization of Effectiveness for Finetuning.

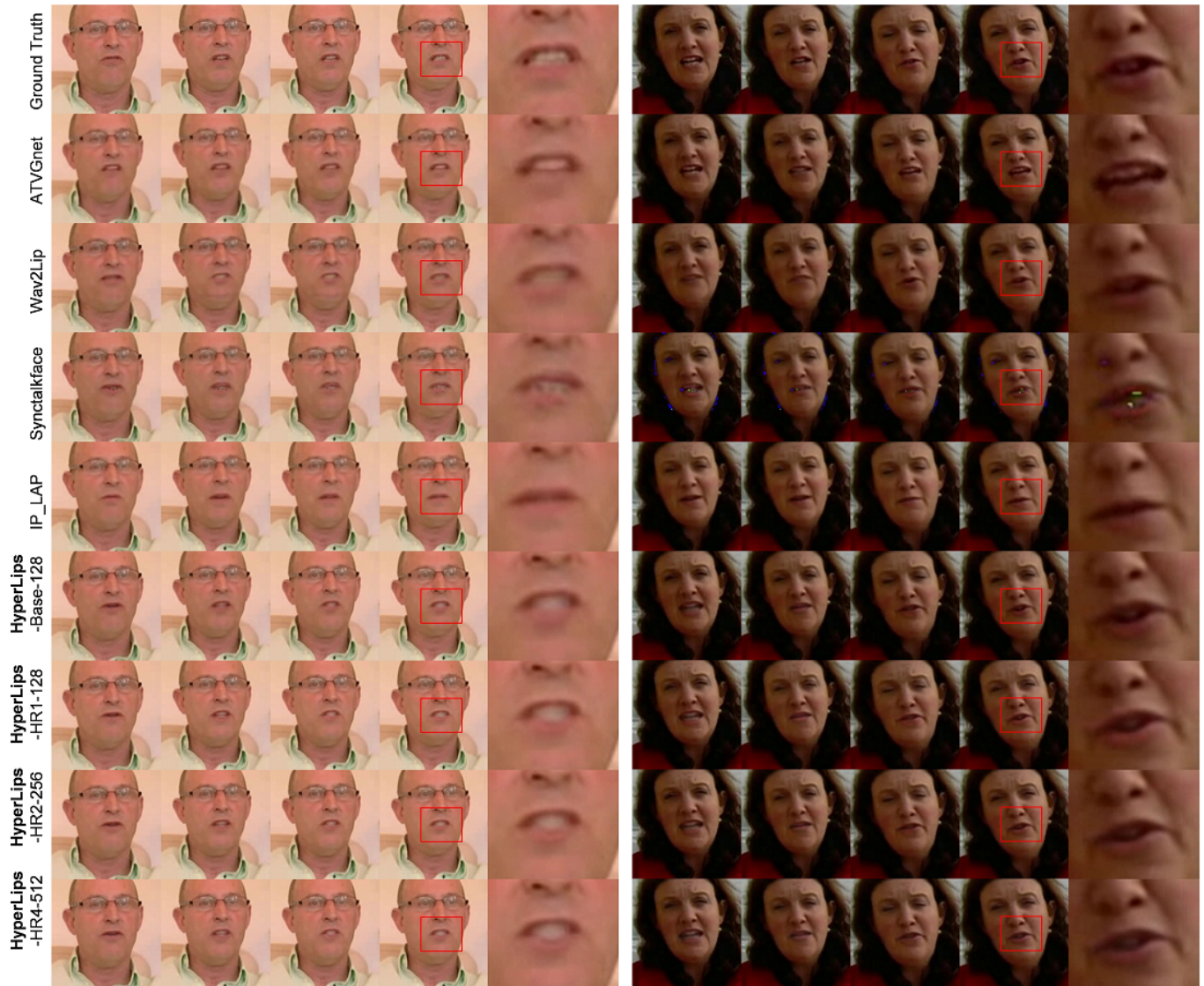


Fig. 19. Qualitative comparisons with state-of-the-art methods on LRS2 [41] datasets.

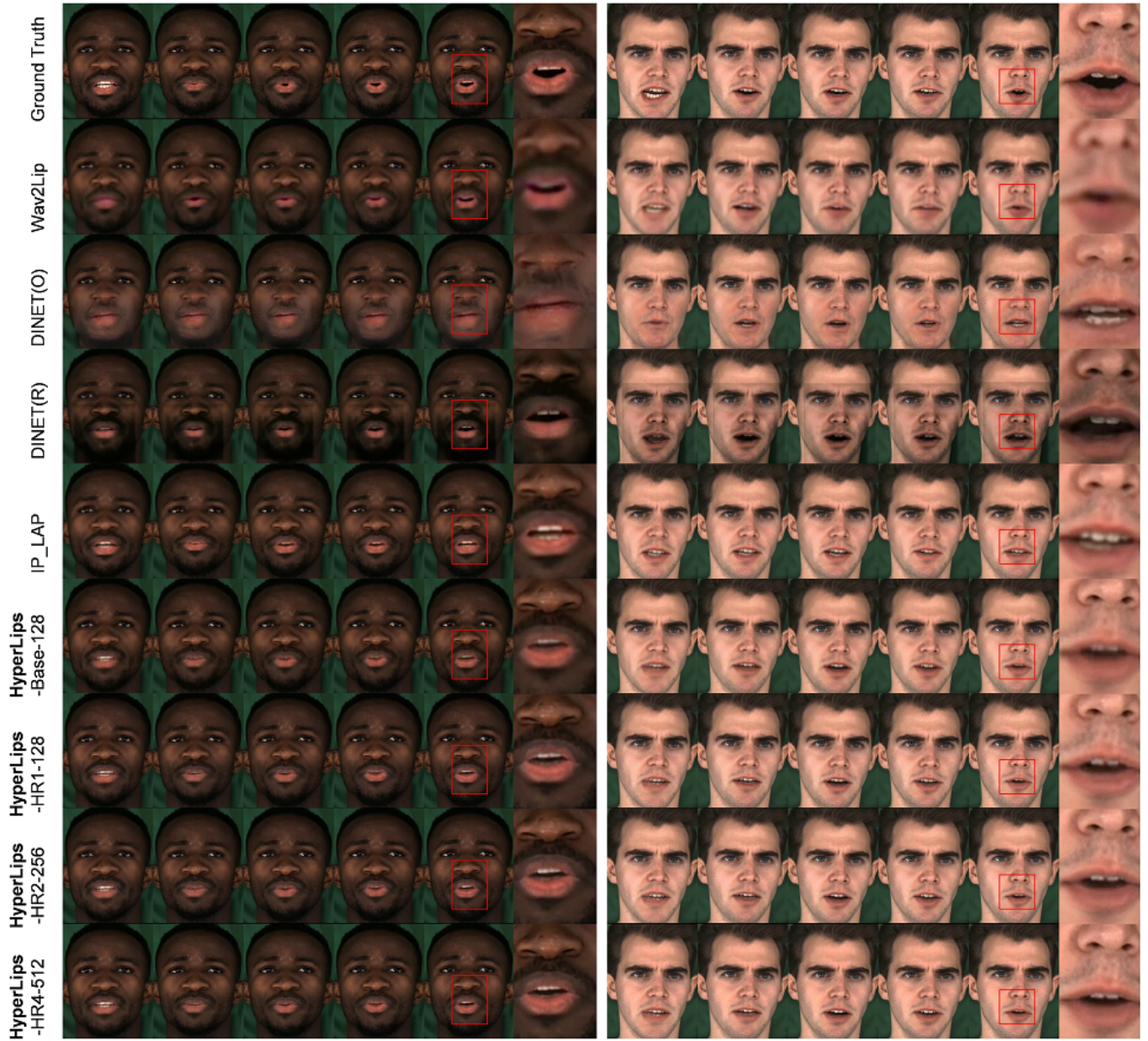


Fig. 20. Qualitative comparisons with state-of-the-art methods on MEAD-Neutral [45] datasets.



Fig. 21. Qualitative comparisons with state-of-the-art methods on MEAD-Neutral [45] datasets.

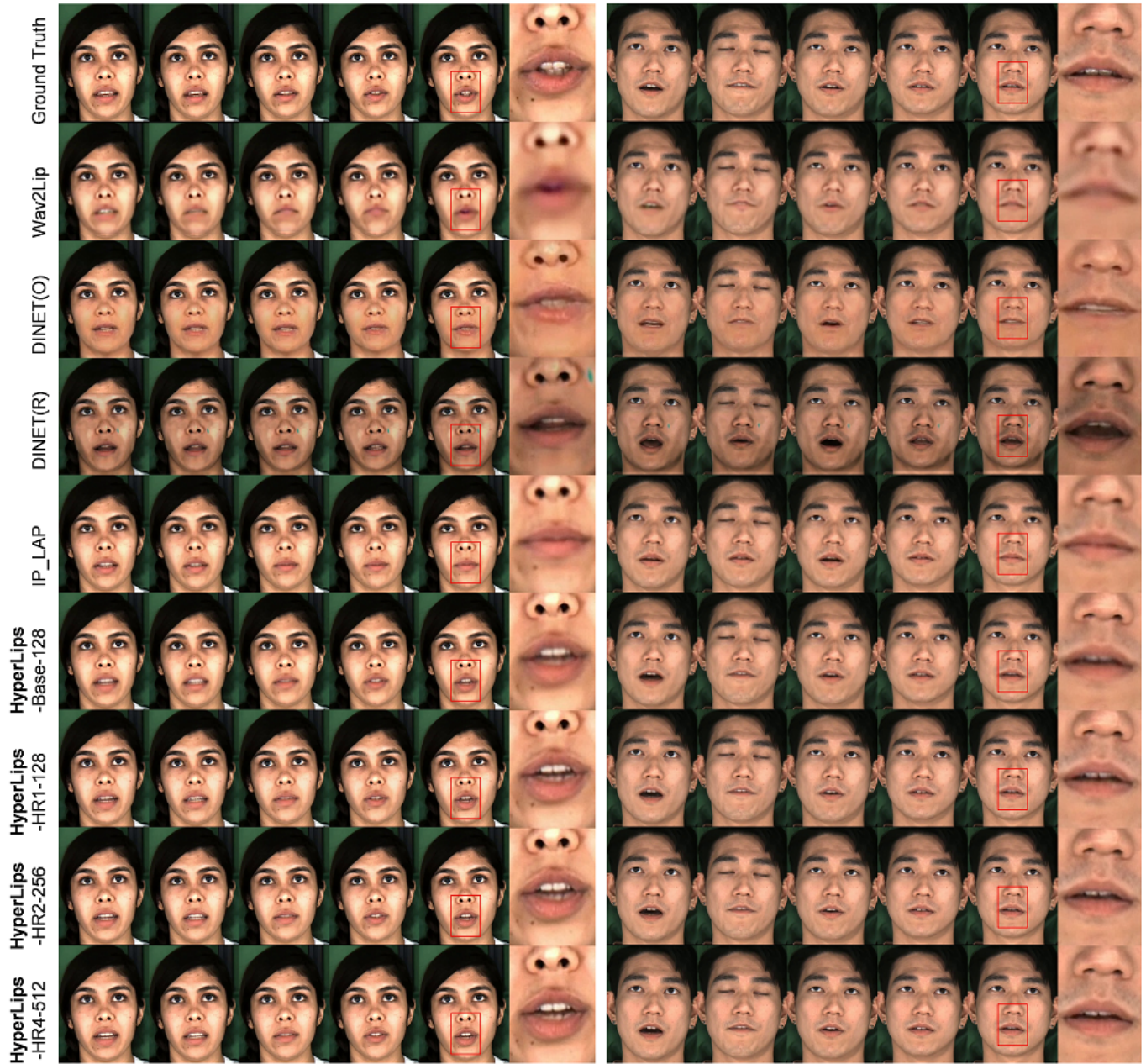


Fig. 22. Qualitative comparisons with state-of-the-art methods on MEAD-Neutral [45] datasets.